Journal of Applied Electrochemistry **29**: 779–788, 1999.

Effect of alumina concentration on the incipience of the anode effect in aluminium electrolysis

H. VOGT
Fachbereich Verfahrens und Umwelttechnik, Technische Fachhochschule Berlin, D-13353 Berlin, Germany

Received 3 July 1998; accepted in revised form 21 October 1998

Key words: aluminium, anode effect, gas evolution, fluid dynamics, two-phase flow

Abstract

The cause of the incipience of the anode effect in alumina reduction cells has long been a controversial issue. The most plausible interpretations are (i) an insufficient release of the gaseous phase from underneath the anode surface together with the action of diminished wettability and (ii) the depletion of oxygen-containing ions at the anode surface to result in the limiting current condition. It is shown by means of a mathematical model that each of these effects may be active. The predominant mechanism depends on the operational conditions. Theoretical results are compared with experimental data.

List of symbols

A	electrode surface area (m^2)
b	Laplace parameter, Equation 21 (m)
c	concentration ($mol\,m^{-3}$)
C_1	parameter of mass transfer, Equation 18 ($A\,m^{-2}$)
C_2	parameter of fluid dynamics, Equation 19 ($A\,m^{-2}$)
d	equivalent bubble diameter (m)
f_G	gas evolution efficiency
f_I	fraction of the current passing through the electrode side walls
F	Faraday constant ($F = 96\,487\,A\,s\,mol^{-1}$)
g	acceleration due to gravity ($m\,s^{-2}$)
H	bubble height (m)
I	total current (A)
j	nominal current density, Equation 2 ($A\,m^{-2}$)
k	mass transfer coefficient ($m\,s^{-1}$)
K	exponent in Equation 22
K_1	multiplier in Equation 36
L	length of electrode edge crossed by bubbles (m)
M	molar mass ($kg\,mol^{-1}$)
n	charge number
p	pressure ($kg\,m^{-1}\,s^{-2}$)
R	universal gas constant ($R = 8.3143\,kg\,m^2\,s^{-2}\,mol^{-1}\,K^{-1}$)
R_0	radius of contact area of adhering bubble (m)
R_s	radius of projected area of adhering bubble (m)
T	temperature (K, °C)
v	bubble velocity ($m\,s^{-1}$)
$\dot{V}_G$	volume flow rate of gas ($m^3\,s^{-1}$)
w	alumina mass fraction in melt
y	coordinate perpendicular to the electrode surface (m)
Sc	Schmidt number, Equation 14
Sh	Sherwood number, Equation 12
Re_G	Reynolds number, Equation 13

Greek symbols

α	angle of inclination
γ	surface tension ($kg\,s^{-2}$)
ε	anodic current efficiency
η	dynamic viscosity ($kg\,m^{-1}\,s^{-1}$)
ϑ	contact angle (°)
Θ	fractional bubble shielding of the electrode surface
υ	stoichiometric number
ρ	density ($kg\,m^{-3}$)
τ_H	shear stress at $y = H$ ($kg\,m^{-1}\,s^{-2}$)

Subscripts

A	alumina
c	critical
G	gas
L	liquid
max	maximum
w	electrode surface
∞	liquid bulk

1. Introduction

In industrial alumina reduction cells with approximately constant current operation, the anode effect manifests itself by a large increase in the cell voltage within some milliseconds [1]. This phenomenon has been known for almost 150 years [2] and its industrial importance has given rise to numerous interpretations of the causes [3]. Recent attempts have taken into account the effect of fluid dynamics on the incipience of the anode effect [4, 5]. The results were compared with measured data of the dependence of the critical current density, associated with the incipience of the anode effect, upon the contact angle, confirming the combined action of fluid dynamics and wettability.

A different view has been taken by Thonstad denying the presence of gas at the anode as a primary cause of the anode effect [6]. He pointed out the action of mass transfer on the incipience of the effect. The anode effect was considered to occur when the melt adjacent to the anode becomes depleted with respect to oxygen-containing ions [3, 7, 8]. Bubbles in contact with the electrode surface contribute to the anode effect in that they result in a higher effective current density than the nominal one [1].

Although the action of fluid dynamics and wettability is not in doubt, the additional action of mass transfer with involvement of gas bubbles deserves attention. Numerous experimental investigations have been carried out on the immediate effect of the alumina concentration on the critical current density. It is the object of the present paper to improve the insight into the mechanisms controlling the onset of the anode effect by an appropriate extension of the above model and quantitative comparison with experimental data.

2. Mass balance

The combined action of fluid dynamics and wettability has been shown on the basis of mathematical models [4, 5]. The key idea was that the volume of gas underneath the electrode is the result of a balance of the rate of gas evolution, on the one hand, and of the conditions of gas release from the underside of the electrode on the other. The rate of gas evolution depends on the total current I according to Faraday's law and the total gas evolution efficiency f_G. This value denotes the fraction of the total amount of electrochemically generated substance (CO_2 + CO) evolved as gas in the form of bubbles grown at the electrode surface [9]. The gas flow rate at the edge of the electrode is controlled by the flow velocity v of bubbles along the electrode surface, by the shape and size of the bubbles with height H. A mass balance of gas generated at, and released from, the electrode results in [5]

$$\frac{j\varepsilon f_G(1-f_I)RT}{(n/\upsilon_G)Fpv\Theta}\frac{A}{HL}=1 \tag{1}$$

with the nominal current density

$$j\equiv\frac{I}{A} \tag{2}$$

Equation 1 takes into account that a fraction f_I of the total current I passes through the side walls of the anode; ε is the anodic current efficiency of the CO_2/CO generating reaction; L is the length of the electrode edge crossed by gas bubbles leaving the underside. The fractional shielding, Θ, denotes the fraction of the electrode area covered (at values of the contact angle $\vartheta \geqslant 90°$) or shielded ($\vartheta \leqslant 90°$) by large gas bubbles [5].

The efficiency of gas evolution, f_G, and Θ are interrelated [9]. At very low values of the current density, where no bubbles are present at the electrode surface, $\Theta \to 0$; the total CO_2 and CO is transferred to the bulk in dissolved form, $f_G \to 0$. At extremely large values of the current density, where the electrode is nearly completely covered with adhering bubbles, $\Theta \to 1$ and the path to liquid bulk is blocked; that is, $f_G \to 1$. For aqueous electrolyte solutions, evaluation of experimental data of various workers suggests a relationship [10]

$$f_G=1-(1-\Theta)^{2.5} \tag{3}$$

Although its applicability to melts and electrode surfaces facing downwards is not confirmed it will be used here in the absence of other information. According to Equation 3 the ratio Θ/f_G is within the limits $0.4 \leqslant \Theta/f_G \leqslant 1$ and may be approximated by

$$\frac{\Theta}{f_G}=\frac{1}{1+1.25(1-\Theta)} \tag{4}$$

Inserting Equation 4 into Equation 1 with elimination of the gas evolution efficiency gives

$$\frac{j\varepsilon(1-f_I)RT}{(n/\upsilon_G)Fpv}\frac{A}{HL}=\frac{1}{1+1.25(1-\Theta)} \tag{5}$$

3. Critical condition

In previous papers [4, 5] the assumption was made that the critical condition for the incipience of the anode

effect is met when the current density reaches a value where the combined action of fluid dynamics and wettability results in a nearly complete gas film on the electrode, $\Theta \to 1$. Then the real current density on the remaining free surface attains large values. When the limiting current density is reached, $j = j_c$, the anodic overpotential increases strongly. The gas evolution efficiency, f_G, approaches unity because the pathway of dissolved gas to the bulk is substantially blocked [5]. When $\Theta/f_G \approx 1$ a critical current density from Equation 1 immediately results:

$$\frac{j_c \varepsilon (1 - f_I) RT}{(n/\upsilon_G) Fpv} \frac{A}{HL} = 1 \tag{6}$$

However, the dependence of the critical current density on the condition $\Theta \to 1$ implies an unnecessary restriction, because the limiting current density, that is, the critical current density associated with the incipience of the anode effect, may be reached at arbitrary values of the fractional shielding Θ, provided the concentration of reactant at the electrode–liquid interface approaches zero. For a more general treatment it is necessary to take account of mass transfer of oxygen-containing ions to the electrode.

4. Mass transfer of reactant

In the available mass transfer equations, the mass transfer coefficient k is, by definition, referred to the total electrode area. In aluminium electrolysis (i.e., under the particular condition of electrode surfaces facing downwards) this is the active electrode area $A(1 - \Theta)$ not blanketed by large bubbles gliding along the surface. The defining equation for k applied to the reactant A (oxygen-containing ions) is, hence,

$$\frac{I(1 - f_I)}{(n/\upsilon_A)F} = kA(1 - \Theta)(c_\infty - c_w) \tag{7}$$

where c_∞ and c_w denote the concentrations of reactant in bulk and in contact with the electrode, respectively. The limiting current density j_c is attained when the interfacial concentration c_w approaches zero, $c_w \to 0$. With introduction of the mass content of A in bulk

$$w_\infty \equiv w = c_\infty \frac{M}{\rho_L} \tag{8}$$

there follows a more general expression of the critical current density

$$j_c = \frac{n}{\upsilon_A} \frac{Fk}{(1 - f_I)} (1 - \Theta) w \frac{\rho_L}{M} \tag{9}$$

Generally, mass transfer of reactant to the electrode is controlled by the combined action of macroconvection and microconvection [11, 12] depending on the current density j. Macroconvection is induced by liquid flow along the electrode, whereas microconvection is due to stirring induced by growing bubbles in the vicinity of the nucleation site [13]. A numerical estimate shows that under the particular conditions of alumina electrolysis, the effect of macroconvection in normal operation is smaller than that of microconvection. The latter mechanism is the predominant one and the only one taken into account in the following estimate. For gas evolving electrodes, the mass transfer coefficient k on the operating area $A(1 - \Theta)$ (not blanketed by large gas bubbles) may be estimated from [9, 13]

$$Sh = 0.93 (Re_G f_G)^{0.5} Sc^{0.487} \tag{10}$$

or in a range $0.2 < \Theta < 0.75$ approximately from

$$Sh = 0.63 Re_G^{0.5} Sc^{0.487} \tag{11}$$

where the dimensionless groups are

$$Sh \equiv \frac{kd}{D} \tag{12}$$

$$Re_G \equiv \frac{j\varepsilon(1 - f_I) RTd\rho_L}{(1 - \Theta)(n/\upsilon_G) Fp\eta_L} \tag{13}$$

$$Sc \equiv \frac{\eta_L}{\rho_L D} \tag{14}$$

and d denotes the diameter of a sphere with the same volume as that of the average bubble detaching from the nucleation site at the electrode surface or disappearing by coalescence with one of the large bubbles. From Equation 11, the mass transfer coefficient, considering Equations 12 and 13, is explicitly

$$k = 0.63 \left[\frac{j\varepsilon(1 - f_I) DRT}{(1 - \Theta)(n/\upsilon_G) Fpd} \right]^{0.5} Sc^{-0.013} \tag{15}$$

4.1. *Critical current density*

Inserting Equation 15 into Equation 9 gives the critical current density,

$$j_c = 0.40\frac{\varepsilon(1-f_I)DRT}{pd}\frac{v_G F}{n}\left(\frac{n}{v_A}\frac{\rho_L}{M}\right)^2 \times Sc^{-0.026}w^2(1-\Theta) \quad (16)$$

Combination with Equation 5 with elimination of Θ finally results in

$$j_c = 0.4\,C_1 w^2\left[\left(1+\frac{5C_2}{C_1 w^2}\right)^{0.5}-1\right] \quad (17)$$

with the abbreviations

$$C_1 \equiv 0.40\frac{\varepsilon(1-f_I)DRT}{pd}\frac{v_G F}{n}\left(\frac{n}{v_A}\frac{\rho_L}{M}\right)^2 Sc^{-0.026} \quad (18)$$

$$C_2 \equiv \frac{(n/v_G)Fpv}{\varepsilon(1-f_I)RT}\frac{HL}{A} \quad (19)$$

Equation 17 is shown for various values of C_2 in Figure 1 together with some experimental lines of various authors. As seen from Figure 2 a variation of C_1 is much less effective than that of C_2. Values of the equivalent diameter d of gas bubbles immediately prior to detachment from the nucleation site or to coalescence with large bubbles are questionable, but this is not detrimental. The variation of C_1 has little effect, particularly under industrial operating conditions.

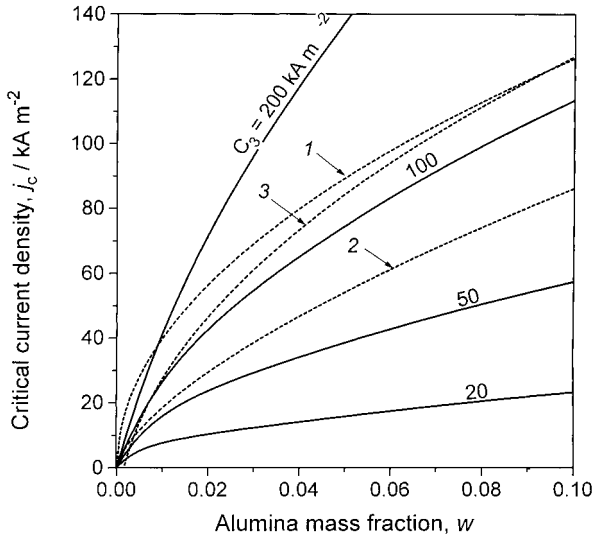

Fig. 1. Equation 17 with $C_1 = 0.4 \times 10^9$ A m^{-2} compared with various empirical equations. Key: (**1**) Equation 32, Beljaev [15]; (**2**) Equation 33, Schischkin [22]; (**3**) Equation 37 for $A = 1\,\text{cm}^2$, Piontelli et al. [26, 27].

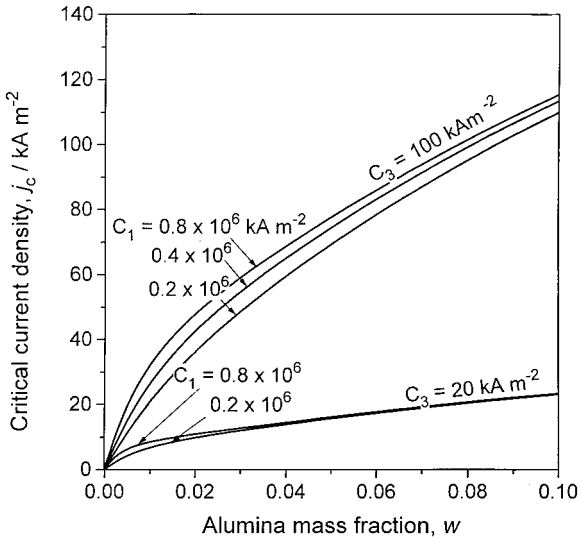

Fig. 2. Equation 17 with various values of C_1.

5. Wettability

Equation 17 does not explicitly show the action of wettability. However, the effect of wettability on the critical current density has been pointed out by various authors, particularly by Beljaev and coworkers [14, 15]. In fact, two variables in Equation 19 depend upon the wettability.

5.1. *Bubble height*

The height H of large bubbles in Equation 19 is affected by the wettability characterized by the contact angle ϑ [5]

$$H = b\sqrt{1+\cos\vartheta} \quad (20)$$

where b denotes the Laplace parameter

$$b \equiv \sqrt{\frac{2\gamma}{(\rho_L-\rho_G)g}} \quad (21)$$

Various experimental investigations [12, 15–17] have demonstrated the effect of the alumina content on the contact angle ϑ, Figure 3. The values coincide satisfactorily at $\vartheta = 127°$ for an alumina content of $w = 0$. They disagree substantially for larger contents, owing to the action of exposure time and electrode material on wettability [15] and may be correlated by

$$\vartheta = \frac{127°}{10^{Kw}} = \frac{0.706\,\pi}{10^{Kw}} \quad (22)$$

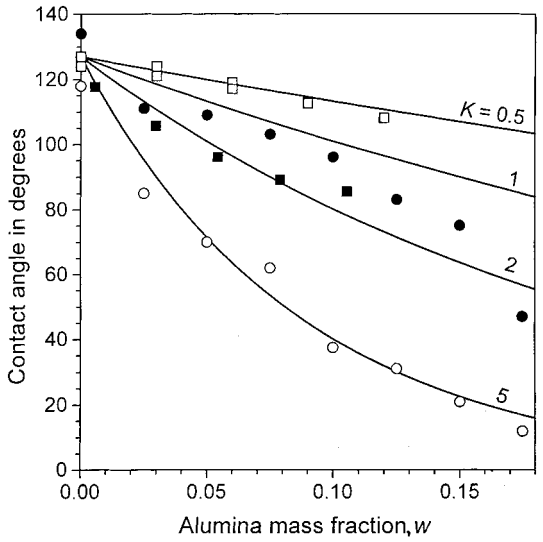

Fig. 3. Contact angle against alumina concentration in the system Na_3AlF_6–Al_2O_3/graphite. Key: (□) Matiasovský et al. [16]; (●) Beljaev et al. [15]; (■) Qiu et al. [17]; (○) Beljaev et al. [14].

with K in the limits $0.5 < K < 5$, Figure 3. Tentatively inserting a value $K = 2$, from Equation 20, gives

$$C_2 = \frac{(n/v_G)Fpv}{\varepsilon(1-f_I)RT}\frac{bL}{A}\left(1+\cos\frac{2.22}{100^w}\right)^{0.5} \tag{23}$$

5.2. *Bubble velocity, v*

For an estimate of the bubble velocity v in Equation 23 some assumptions are required. A balance of forces acting on a gas bubble underneath a surface facing downwards, taking account of buoyancy, controlled by the angle of inclination α of the rounded off edge, of shear stress τ_H acting on the gas–liquid interface of large bubbles, and of the wetting force, gives [5]

$$v = \frac{(\rho_L-\rho_G)g\ \sin\ \alpha}{3\eta_G}H^2 \times\left\{1+\frac{1.5\,\tau_H}{H(\rho_L-\rho_G)g\ \sin\ \alpha}\left[\frac{1-4\gamma R_0\Delta\vartheta\ \sin\ \vartheta}{\pi R_s^2\tau_H}\right]\right\} \tag{24}$$

The maximum height $H = H_{max}$ of the bubble is given by $\vartheta \to 0$, Equation 20. The resulting maximum bubble velocity is

$$v_{max} = \frac{(\rho_L-\rho_G)g\sin\alpha}{3\eta_G}H_{max}^2 \times\left[1+\frac{1.5\,\tau_H}{H_{max}(\rho_L-\rho_G)g\ \sin\ \alpha}\right] \tag{25}$$

The ratio is, hence,

$$\frac{v}{v_{max}} = \left(\frac{H}{H_{max}}\right)^2 \times\left\{\frac{1+\frac{1.5\tau_H}{H(\rho_L-\rho_G)g\ \sin\ \alpha}\left[1-\frac{4\gamma R_0\Delta\vartheta\ \sin\vartheta}{\pi R_s^2\tau_H}\right]}{1+\frac{1.5\tau_H}{H_{max}(\rho_L-\rho_G)g\ \sin\ \alpha}}\right\} \tag{26}$$

The shear stress τ_H may be positive or negative, depending on the operation conditions. As an approximation for the sake of simplicity, it is reasonable to suppress the term in the square bracket:

$$\frac{v}{v_{max}} = \frac{H}{H_{max}}\left\{\frac{1+\frac{H(\rho_L-\rho_G)g\ \sin\ \alpha}{1.5\tau_H}}{1+\frac{H_{max}(\rho_L-\rho_G)g\ \sin\ \alpha}{1.5\tau_H}}\right\} \tag{27}$$

At small values of the angle of inclination, α, of the anode surface, Equation 27 approaches

$$\frac{v}{v_{max}} = \frac{H}{H_{max}} \tag{28}$$

to be used as a general approximation. Considering Equation 20 gives

$$\frac{v}{v_{max}} = \sqrt{\frac{1+\cos\vartheta}{2}} \tag{29}$$

Equation 23 then takes the form

$$C_2 = C_3\left(1+\cos\frac{2.22}{100^w}\right) \tag{30}$$

with the abbreviation

$$C_3 \equiv \frac{(n/v_G)Fpbv_{max}}{\sqrt{2}\varepsilon(1-f_I)RTA/L} \tag{31}$$

The critical current density is to be calculated from Equation 17 with the abbreviations C_1 and C_2 from Equations 18, 21, 30 and 31. The maximum bubble velocity v_{max} may be estimated on the basis of measured values.

6. Comparison with experimental data

Two extremely different sets of experimental data will be used to test Equation 17: results obtained from industrial cells [1] and from a small laboratory cell with forced flow [7], both for reduction of Al_2O_3. These data differ not only in the size of the electrodes and the operational conditions but also in the results. In Thonstad's labo-

ratory cell, the anode effect occurred at a critical current density which was about 10 times the value observed in industrial cells at the same alumina content.

6.1. *Laboratory cell*

Thonstad [7] investigated the critical current density at a vertical anode of 16 mm height and 6.25 mm width in the current density range $j_c = 0$ to $180\,kA\,m^{-2}$. The bubbles left the anode across its height with the length $L = 16\,mm$, resulting in $A/L = 0.00625\,m$. The melt was circulated with a circumferential speed of the rotating cylinder of $0.274\,m\,s^{-1}$. With an interpolar distance of about 10 mm, the velocity of bubbles with maximum height is $v_{max} \approx 0.13\,m\,s^{-1}$. The break-off diameter in Equation 18 was set as $d = 40 \times 10^{-6}\,m$ with reference to bubble diameters in aqueous solutions [18]. Further operational data and properties of the melt used for calculation of the parameters C_1 and C_2 are given in Table 1.

6.2. *Industrial cell*

The critical current density for industrial cells is much lower. The anode effect occurs at values of the alumina content $w = 1$ to 2% at a current density $j_c = 7500\,A\,m^{-2}$ [1]. The range agrees with that found by Beljaev [14]. For typical prebaked anode dimensions, $1.35 \times 0.75\,m^2$ [19], the resulting ratio is $A/L = 0.24\,m$ (assuming that the gas leaves the underside of each anode across the total edge). The velocity of the melt was estimated from values given in the literature [20, 21]. The maximum velocity of a bubble with maximum height near the edge was set as $v_{max} = 0.3\,m\,s^{-1}$. The break-off diameter was again set as $d = 40\,\mu m$.

Equation 17 is plotted for both the laboratory and the industrial cell in Figure 4.

7. Discussion

Equation 17 was checked in comparison with published experimental data obtained from two very different alumina reduction cells. The electrode areas of the cells differed by a factor of 10^4. At an alumina content of $w = 1.5\%$ the critical current density of the industrial cell was $j_c = 7.5\,kA\,m^{-2}$, that of the laboratory cell was $j_c = 55\,kA\,m^{-2}$. The amazingly good agreement between theory and the available experimental data, Figure 4, confirms the view that the critical current density associated with the anode effect is identical with the limiting current density *at a certain bubble coverage*. Particularly the idea of several workers to attribute the onset of anode effect *directly* to the action of isolating surface layers appears to be obsolete.

Some of the data used are questionable. The uncertainty with respect to the detachment diameter d in Equation 18 is not detrimental as shown above, but the approximation of Equation 26 by Equation 28 is uncertain, and the bubble height used in Equation 20 is the equilibrium value and may differ from that of gliding bubbles [25]. However, Equation 17 appears appropriate to elucidate the mechanism leading to the anode effect.

Figure 1 also shows some empirical equations. On the basis of experimental data obtained with laboratory cells, Beljaev [15] proposed a relationship

$$j_c \sim w^{0.5} \tag{32}$$

Table 1. Data used for calculations

Quantity	Units	Industrial cell (Thonstad et al. 1984 [1])	Laboratory cell (Thonstad 1967 [7])
A	m^2	1.0	10^{-4}
A/L	m	0.24	0.00625
n/v_A	–	6	6
n/v_G	–	3.5	3.5
f_I	–	0.2	0
ε	–	0.9	0.9
v_{max}	$m\,s^{-1}$	0.3	0.13
d	m	40×10^{-6}	40×10^{-6}
T	°C	1000	1010; 1020
p	Pa	105000	10^5
ρ_L	$kg\,m^{-3}$	2050	2050
γ	$kg\,s^{-2}$	0.14	0.14
D	$m^2\,s^{-1}$	1.5×10^{-9}	1.5×10^{-9}
M_A	$kg\,mol^{-1}$	0.102	0.102
η_L	$kg\,m^{-1}\,s^{-1}$	2.7×10^{-3}	2.7×10^{-3}

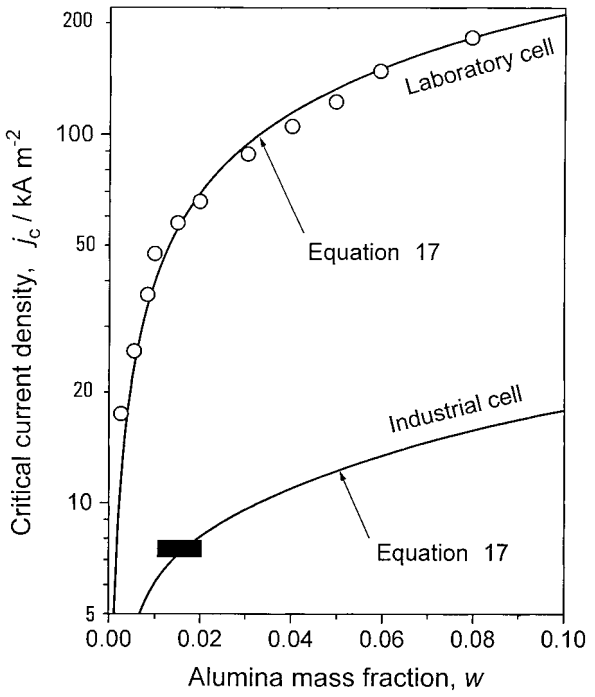

Fig. 4. Comparison of Equation 17 with experimental data. Key: (■) industrial cells, Thonstad et al. [1]; (○) laboratory cell, Thonstad [7].

whereas Schischkin [22] proposed

$$j_c \sim w^{2/3} \tag{33}$$

Qiu and Zhang [23, 24] approximated their data by

$$j_c = (2500 + 2.75 \times 10^6 w)\ \mathrm{A\,m^{-2}} \tag{34}$$

in the range $w < 0.02$ and by

$$j_c = 4 \times 10^5 w^{0.5}\ \mathrm{A\,m^{-2}} \tag{35}$$

in the range $0.02 < w < 0.04$. These relationships and numerous other experimental equations [3, 4], exhibit behaviour which is in qualitative agreement with equation (17).

The ratio A/L in Equation 31 has the dimension of length and may be related to the electrode area by

$$\frac{A}{L} = K_1\sqrt{A} \tag{36}$$

The multiplier K_1 depends on the shape of the electrode area, $K_1 = 0.23$ to 0.25 for the usual rectangular electrodes in industrial cells. The effect of the electrode size on the critical current density has already been recognized by Piontelli and coworkers [26, 27]. Their empirical equation for $j_c(\mathrm{A\,cm^{-2}})$ is

$$j_c = \left[5.5 + 0.018\left(\frac{T}{^\circ\mathrm{C}} - 1050\right)\right]\left(\frac{A}{\mathrm{cm^2}}\right)^{-0.1} \times (10w^{0.5} - 0.4) \tag{37}$$

although later considered dubious [3], takes account of the area in at least a qualitatively correct way. Equation 37 is shown in Figure 1. Recently, Richards deduced from experimental data that the electrode size affects the fractional shielding Θ [25]. This is a further confirmation of the action of the electrode area on the onset of the anode effect as seen from Equation 19.

Approximating Equation 3 simply by

$$\frac{\Theta}{f_G} = 0.4 + 0.6\,\Theta \tag{38}$$

shows an interesting result. Combining Equations 1, 16 and 38 gives the simple relationship

$$\frac{1}{j_c} = \frac{1}{2C_1w^2/3} + \frac{1}{C_2} \tag{39}$$

instead of Equation 17. The two terms on the right hand side may be interpreted as resistances, both depending on the alumina content w. The first term accounts for the concentration of reactant at the electrode-liquid interface, expressing the effect of mass transfer on the limiting current density; the second takes account of the combined action of wetting and fluid dynamics. Equation 39 is shown in Figure 5 with the data for the industrial cell treated above together with the experimental value of the critical current density. Furthermore, the inverse of the above two resistances are shown. It is seen that $2/3C_1w^2$ forms the asymptotic line of Equation 39 for $w \to 0$ and C_2 that for $w \to \infty$. When the sum of both resistances equals the inverse of the actual current density, the anode effect occurs.

The result illustrates that the incipience of the anode effect is controlled by two different effects. At low values of alumina concentration mass transfer is the controlling parameter. Fluid dynamics and wetting properties have no effect. The situation is completely different at high alumina contents. Here fluid dynamics and wettability control the incipience of the anode effect by increasingly lowering the active electrode area. These circumstances are clearly visible from Figure 6 where the fractional shielding Θ is plotted after combination of Equations 1 and 3:

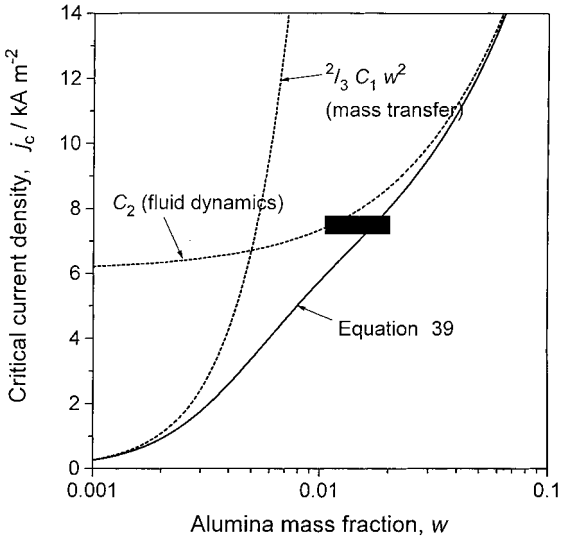

Fig. 5. Equation 39 and its asymptotic lines of the action of pure mass transfer and pure fluid dynamics, respectively. Key: (■) experimental for industrial cells [1].

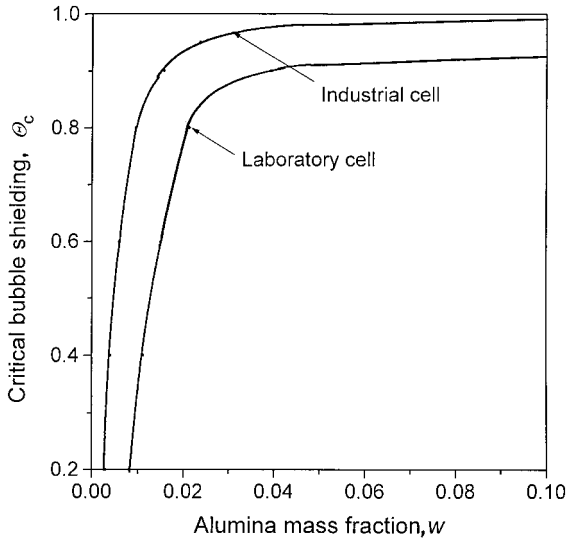

Fig. 7. Critical fractional shielding. Key: (1) industrial cells [1]; (2) laboratory cell [7]. Data from Table 1.

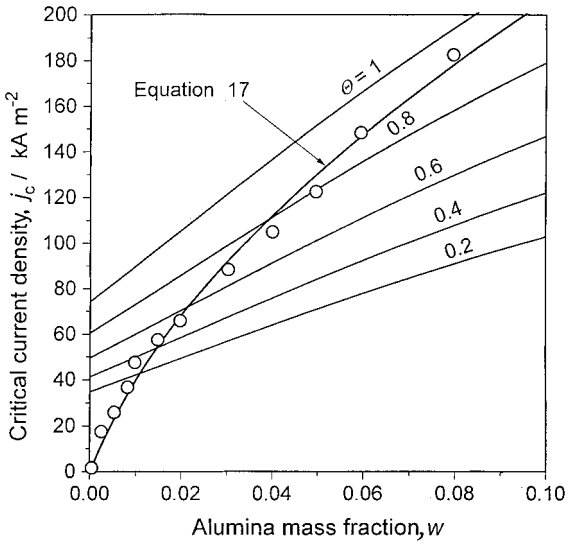

Fig. 6. Fractional bubble shielding, Θ, during the incipience of the anode effect. Equations 40 and 17 applied to the conditions of Thonstad's laboratory cell. Key: (○) laboratory cell [7].

$$j = \frac{C_2\Theta}{1-(1-\Theta)^{2.5}} \tag{40}$$

with C_2 for the laboratory cell of the Thonstad experiment [7]. The intersections of Equations 17 and 40 indicate the critical fractional shielding. These data are shown separately for both the laboratory cell and the industrial cell in Figure 7. It is seen from Figures 5 and 6 that the bubble coverage at the onset of the anode effect increases with the critical current density. The impact of fluid dynamics increases with increasing alumina content w, and the action of fluid dynamics is commonly the predominant mechanism as also seen from Figure 5. At small values of Θ, mass transfer is predominant. The previous interpretation of the mechanism controlling the onset of the anode effect [5] must be restricted to the particular condition of large alumina contents.

As seen from Figure 6, at constant current density, the fractional shielding Θ is directly interrelated to the alumina content w in such a way that decreasing values of w result in increasing values of Θ. This explains a finding of Richards calculated from experimental data of the anodic overpotential [25]. For a 18.8 m^2 Söderberg cell operated at 150 kA the fractional shielding Θ increased from 0.11 to 0.75 as the alumina content decreased from 5 to 2%.

Using a critical current density is a common practice, but not necessarily appropriate in cases of predominant fluid dynamics. It is seen from Equation 1 that not the critical current density, but a critical current, is the controlling parameter. More strictly, a flow rate of evolved gas

$$\dot{V}_G = \frac{I\varepsilon(1-f_I)RT}{n/\upsilon_G Fp} \tag{41}$$

may be considered the controlling parameter, which becomes a critical one if the gas release is not strong

enough to prevent gas accumulation of such an extent that the resulting effective current density approaches the limiting one. This is affected by the flow velocity and the form of the bubbles. Wettability acts on H and v as seen from Equations 23 and 29.

8. Conclusion

The agreement of the results of the theoretical model with experimental and industrial data suggests the following interpretation. Generally, the condition of the incipience of the anode effect is met when the limiting current density associated with supply of reactant is attained. If the interfacial concentration of reactant approaches zero, $c_w \to 0$, the anode effect occurs. The critical current density is identical with the limiting current density (cf. Equation 9):

$$j_c \equiv \frac{I_c}{A} = \frac{n}{\upsilon_A}\frac{F}{(1-f_I)}(1-\Theta)kc_\infty \qquad (42)$$

Equation 42 immediately shows that each of two limiting conditions is sufficient to initiate the anode effect. Either the mass transfer group (kc_∞) of reactant or, under constant current conditions, the active electrode area $A(1-\Theta)$ approaches zero.

At small values of the bulk concentration, $c_\infty \to 0$, small values of the current density are sufficient to attain the limiting current density condition, as seen from Equation 42. At small current densities, the electrode surface is covered by only a few bubbles. Then the expression $(1-\Theta)$ does not differ significantly from unity. Therefore, the limiting current density is virtually solely controlled by the product kc_∞, that is, mass-transfer controlled (diffusion controlled) in agreement with Thonstad's view of 1967 [7]. The anode effect simply starts as the result of the depletion of reactant at the electrode, virtually irrespective of a diminution in the active electrode area.

Increasing current density results in a decrease in the active electrode area (i.e., the area not blanketed by bubbles) for two reasons. In addition to the increasing rate of evolved gas, the increasing actual current density $j/(1-\Theta)$ activates additional bubble nucleation sites. The fractional shielding Θ is controlled by the balance of gas evolution and gas release. As seen from Equation 1 the relevant parameters are the current (not the nominal current density), the size and shape of the electrode, A/L, the height H and the velocity v of the bubbles. The latter two are controlled by wettability, (Equations 20 and 29). At large values of the nominal current density, the mass transfer coefficient k does not produce an effect. Although an increase in the current density is accompanied by an increase in k, the increase is always smaller than that in the current density, Equation 15. So arbitrarily large values of k would not prevent the anode effect when the fluid dynamic conditions induce blockage of the electrode area by bubbles, $\Theta \to 1$. Then the onset of the anode effect is no longer mass transfer controlled but the result of the common action of fluid dynamics and wettability as previously shown [4, 5]. The action of wettability had already been pointed out in 1916 by Oesterheld and Brunner [28] and later by others [29, 30].

In fact, none of these limiting cases is separately active. The anode effect occurs at values $c_\infty > 0$ and $\Theta < 1$. The findings suggest that the incipience of the anode effect is the result of the common action of mass transfer, fluid dynamics and wettability. Whether the anode effect is controlled by mass transfer or by fluid dynamics and wettability depends upon the operating conditions.

References

1. J. Thonstad, F. Nordmo, A.H. Husøy, K. Ø. Vee and D.C. Austrheim, *in* 'Light Metals 1984', edited by J.P. McGeer (Warrendale 1984), p. 825.
2. R. Bunsen, [Poggendorff's] *Ann. Physik* **92** (1854) 648.
3. K. Grjotheim, C. Krohn, M. Malinovský, K. Matiasovský and J. Thonstad, 'Aluminium Electrolysis' (Aluminium-Verlag, Düsseldorf, 1977; 2nd edn. 1982).
4. H. Vogt, *Electrochim. Acta* **42** (1997) 2695.
5. H. Vogt, *J. Appl. Electrochem.* **29**:2 (1999) 137.
6. J. Thonstad, F. Nordmo and K. Vee, *Electrochim. Acta* **19** (1973) 27.
7. J. Thonstad, *Electrochim. Acta* **12** (1967) 1219.
8. J. Thonstad, F. Nordmo and J.K. Rødseth, *Electrochim. Acta* **19** (1974) 761.
9. H. Vogt, *Electrochim. Acta* **29** (1984) 167 and 175.
10. H. Vogt, *J. Electrochem. Soc.* **137** (1990) 1179.
11. H. Vogt, *Electrochim. Acta* **32** (1987) 633.
12. H. Vogt, *Electrochim. Acta* **38** (1993) 1421.
13. K. Stephan, H. Vogt, *Electrochim. Acta* **24** (1979) 11.
14. A.I. Beljaev, M. B. Rapoport and L.A. Firsanova, 'Metallurgie des Aluminiums', vol. 1 (Verlag der Technik, Berlin 1956) pp. 121 *ff*.
15. A.I. Beljaev, E.A. Zhemchuzhina and L.A. Firsanova, 'Physikalische Chemie geschmolzener Salze. (Dt. Verlag für Grundstoffindustrie, Leipzig, 1964).
16. K. Matiasovský, M. Paucirova and M. Malinovský, *Chem. Zvesti* **17** (1963) 181.
17. Z. Qiu, C. Wei and M. Chang, 'Light Metals 1982', edited by J.E. Andersen (Metallurgical Society AIME, Warrendale, 1982), p. 279.
18. H. Vogt, *in* 'Comprehensive Treatise of Electrochemistry' (edited by E. Yeager, J.O'M. Bockris, B.E. Conway, S. Sarangapani, vol. 6 (Plenum, New York, 1983), p. 455.
19. J. Zoric, I. Roušar and J. Thonstad, *J. Appl. Electrochem.* **27** (1997) 916.

20. A.V. Nikitin, V.A. Kryukovskii, and N.S. Mikhalitsin, *Tsvetn. Met.* **16** (8) (1975) 31; *Sov. J. Non-Ferrous Met.* **16** (8) (1975) 37.
21. A. Solheim, S.T. Johansen, S. Rolseth, and J. Thonstad, *J. Appl. Electrochem.* **19** (1989) 703.
22. V. Schischkin, *Z. Elektrochemie* **33** (1927) 83.
23. Qiu Z. and Zhang M., *Aluminium* **61** (1985) 911.
24. Qui Z. and Zhang M., *Electrochim. Acta* **32** (1987) 607.
25. N.E. Richards, 'Light Metals 1998', edited by B. Welch (Warrendale, 1998), p. 521.
26. R. Piontelli, B. Mazza and P. Pedeferri, *Electrochim. Acta* **16** (1965) 1117.
27. R. Piontelli, B. Mazza and P. Pedeferri, *Metallurg. Ital.* **57** (2) (1965) 1.
28. G. Oesterheld and H. Brunner, *Z. Elektrochemie* **22** (1916) 38.
29. K. Arndt and H. Probst, *Z. Elektrochemie* **29** (1923) 323.
30. G.-E. Taylor, *Trans. Amer. Electrochem. Soc.* **47** (1925) 301.